Gold Nano-Popcorn Based Targeted Diagonosis, Nanotherapy Treatment and In-Situ Monitoring of Photothermal Therapy Response of Prostate Cancer Cells Using Surface Enhanced Raman Spectroscopy

Wentong Lu, **Anant Kumar Singh**, **Sadia Afrin Khan**, **Dulal Senapati**, **Hongtao Yu**, and **Paresh Chandra Ray**[*]
Department of Chemistry, Jackson State University, Jackson, MS, USA

Abstract

Prostate cancer is the second leading cause of cancer-related death among the American male population and the cost of treating prostate cancer patients is about $10 billion/year in the US. Current treatments are mostly ineffective against advanced stage prostate cancer disease and are often associated with severe side effects. Driven by the need, in this manuscript, we report multifunctional nanotechnology-driven gold nano-popcorn based surface enhanced Raman scattering (SERS) assay for targeted sensing, nanotherapy treatment and in-situ monitoring of photothermal nanotherapy response during the therapy process. Our experimental data show that in the presence of LNCaP human prostate cancer cell, multifunctional popcorn shape gold nanoparticle forms several hot spots and provides a significant enhancement of the Raman signal intensity by several orders of magnitude (2.5×10^9). As a result, it can recognize human prostate cancer cell in 50 cells level. Our results indicate that the localized heating that occurs during NIR irradiation is able to cause irreparable cellular damage of the prostate cancer cell. Our in-situ time dependent results demonstrates for the first time that by monitoring SERS intensity change, one can monitor photo thermal nanotherapy response during therapy process. Possible mechanisms and operating principle of our SERS assay have been discussed. Ultimately, this nanotechnology driven assay could have enormous potential applications in rapid, on-site targeted sensing, nanotherapy treatment and monitoring of nanotherapy process which is critical to providing effective treatment of cancer disease.

Introduction

Prostate cancer is the most common malignancy among American men and it is the second leading cause of cancer-related death among the American male population and the cost of treating prostate cancer patients can be $10 billion/year in the US [1-5]. In 2009, an estimated 192,000 new cases of prostate cancer were diagnosed and about 27,000 men died from the disease [1-5]. Current treatment including surgery, radiation therapy, and chemotherapy are mostly ineffective against advanced stage prostate cancer disease and also often associated with severe side effects [1-10]. As a result, new approaches to treat prostate cancer that do not rely on traditional therapeutic regimes, is very urgent for public health as well as world economy [5-15]. Recently, gold nanoparticles of different sizes and shapes with optical properties tunable in the near-infrared (NIR) region have been exploited for the hyperthermic destruction of cancer cells and upon successful trial, they can be used as drugs

paresh.c.ray@jsums.edu, Fax: 601-979-3674.

in photothermal nanotherapy [11–30]. With the ability to generate high temperatures at a desired site with externally tunable control of gold nanoparticles combined with biocompatibility and low toxicity, perhaps the greatest promise of impact of gold nanotechnology for society will be the therapeutic challenges of cancer [11–30]. Ultimately photo-thermal nanotherapy may enter into clinical oncology. As a result, currently there is an urgent need of techniques for monitoring nanotherapy response to tumor during the photothermal nanotherapy process. Driven by the need, in this manuscript, we report multifunctional gold nano-popcorn based surface enhanced Raman scattering (SERS) approach [31–39] for targeted sensing, nanotherapy treatment and in-situ monitoring photothermal nanotherapy response during the therapy process. Ideally, our nanotechnology based reported assay would have enormous potential for providing effective, noninvasive treatment of cancer *in vivo via* photothermal therapy.

Due to the established synthetic protocols for the controlled preparation of colloidal nanostructures and unique optical properties of nanomaterials, since last couple of years several groups have been developing suitable nanomaterials for cancer imaging and therapy [11–50]. In nano-popcorn, the central sphere acts as an electron reservoir while the tips are capable of focusing the field at their apexes which will provide sufficient field of enhancement. As a result, in popcorn shape gold nanoparticle, the low cross-section Raman signals can be amplified several orders of magnitude particularly in narrow nanoscaled corners and edges [51–52]. This very high sensitivity afforded by surface enhanced Raman spectroscopy (SERS), along with the highly informative spectra characteristic of Raman spectroscopy, will provide nano-popcorn based SERS to be unique for ultrasensitive biological analysis. Using these unique SERS properties, we report for the first time that multifunctional gold nano-popcorn driven SERS assay for targeted sensing, phtothermal therapy treatment and monitoring in-situ nanotherapy progress of prostate cancer cell. In our study, we have used a well-characterized human prostate cancer cell line LNCaP which expresses a high level of prostate-specific membrane antigen (PSMA) [24–25] relative to normal cells of the prostate and it has been shown that PSMA expression increases with clinical stag. There is mounting evidence that normal tissue including epithelium of the duodenum, kidney, endometrium, and breast also expresses PSMA[30]. As a result, immunophenotypic analyses of cancer cells using antibody probes for specific surface antigens can dramatically influence selectivity, and resulting in false positive signals [6–20]. Target cell-specific aptamers have the potential to serve as molecular probes for specific recognition of the cancerous cells, but unfortunately, aptamers have weak binding affinity and thus low signal in molecular imaging, limiting their ability for highly sensitive detection of cancer cells [6–30]. Also during the early stages of cancer development, cancer cells will have a very low density of target membrane proteins for recognition of specific cancer cell [53–55]. As a result, single-aptamer/antibody binding will not be enough to detect early stage cancer development and multivalent binding is usually considered to be essential for early stage disease diagnostics.[1–30] For selective sensing, therapy and monitoring of therapy progress, we have conjugated gold nano-popcorn by multiple PSMA specific targets and these are 1) anti PSMA antibody and 2) Raman dye (Rh 6G) attached A9 RNA anti-PSMA aptamer [24–25]. Rh 6G modified RNA aptamers covalently attached to the surface serve a dual function as targeting molecules and as Raman dye carrying vehicle.

Materials and Experiments

Hydrogen tetrachloroaurate (HAuCl$_4$.3H$_2$O), NaBH$_4$, sodium citrate, cystamine dihydrochloride, cetyl trimethylammonium bromide (CTAB) were purchased from Sigma-Aldrich and used without further purification. Monoclonal anti-PSMA antibody were purchased from Thermo Fisher Scientific, 3′-SH and 5′-Rh6G modified A9 RNA aptamer were purchased from Midland Certified Reagent. The human prostate cancer cell line

LNCaP which overexpresses a high level of prostate-specific membrane antigen (PSMA), was obtained from the American Type Culture Collection (ATCC, Rockville, MD). PSMA negative human prostate cancer cell line (PC-3) [24–25] was also purchased from ATCC. Human skin HaCaT keratinocytes, a transformed human epidermal cell line, was obtained from Dr. Norbert Fusenig of the Germany Cancer Research Center, Heidelberg, Germany.

Synthesis of Popocorn Shape Gold Nanoparticle

Our gold nano-popcorn synthesis was achieved through a two-step process, using seed-mediated growth. In the first step, very small, reasonably uniform, spherical seed particles were generated using tri-sodium citrate as stabilizer and sodium borohydride as strong nucleating agent. In the second step, we have used ascorbic acid as weak reductant as well as CTAB as shape templating surfactant so that the seeds can grow into larger particles of particular morphology we desired. The ascorbic anions transfer electrons to the seed particles, which will reduce gold ions to form gold shell, which grows into different shapes in the presence of CTAB. Gold spherical seeds were synthesized by mixing aqueous solutions of hydrogen tetrachloroaurate (III) hydrate with trisodium citrate in 20ml double distilled deionized water (18MΩ) where the final concentration of $HAuCl_4.3H_2O$ was at 2.5×10^{-4}M and the concentration of trisodium citrate was 10^{-4}M. An ice cooled, freshly prepared aqueous solution of sodium borohydride, $NaBH_4$ (0.1M, 60μL) was then added under vigorous stirring. Solution turned pink immediately after the addition of $NaBH_4$, which became red after keeping the solution in dark for overnight. Nano-seeds exhibit absorption spectra with a maximum at 510 nm, which corresponds to 4.3 nm seed, which has been confirmed by TEM.

After that, nano-popcorn was synthesized using the seed mediated growth procedure in the presence of CTAB. For this preparation, we have dissolved 0.05gm CTAB in 46.88ml H_2O by sonication in a small vial and then we added 2ml 0.01M $HAuCl_4.3H_2O$ under constant stirring. Next 0.3 ml 0.01M $AgNO_3$ is added to the solution to mix properly. After that, we added 0.32ml 0.1M ascorbic acid drop wise as a reducing agent. The solution turned to colorless from yellow. To this colorless solution, we instantly added 0.5ml gold nano-popcorn seed at a time and mixed the solution for next 2 min. Color changed immediately and became blue within 2 min, which indicates the formation of popcorn nanostructures. JEM-2100F transmission electron microscope (TEM) and UV-visible absorption spectrum were used to characterize the nanoparticles (as shown in Figure 1). This popcorn shape gold nanoparticle has only one plasmon bond like spherical gold nanoparticle but their λ_{max} shifted about 60 nm, in comparison to the spherical gold nanoparticle of same size. Popcorn shape gold nanoparticle concentration was measured using plasmon absorption peak at 580 nm given the popcorn shape nanoparticle extinction coefficient is 4.6×10^9 M^{-1} cm^{-1}. Extinction coefficient was measured by using ICP analysis to quantitatively determine the gold concentration in nanoparticle solution and nanoparticle volume measured by TEM. Similar method has been used by El-Sayed et. al [56] and Murphy et. al[57] for the measurement of the extinction coefficients of different shape gold nanoparticles. This experiment has been performed 5–6 times and average values are reported in this manuscript.

Preparation of Multifunctional Popcorn Shape Nano-conjugates

As we discussed in the last section, popcorn shape gold nanoparticles were synthesized using seed-mediated growth procedure in the presence of CTAB. The above procedure produced popcorn shape gold nanoparticle with CTAB coating. CTAB is known to be cytotoxic and as a result, it will not be ideal for in vivo diagnosis. Furthermore, since CTAB is positively charged at physiological pH and will be able to attract negatively charged proteins easily. As a result, CTAB coated popcorn shape gold nanoparticle can face severe

nonspecific binding problems. To overcome this problem, we have modified the oval shape gold nanoparticle surface by -3′-SH and 5′-Rh6G modified –A9 RNA aptamers capture oligonucleotides, -A9 RNA aptamers and cystamine dihydrochloride (as shown in Scheme 1) using reported method [26,40,50]. -SH labeled RNA capture oligonucleotides & -A9 RNA aptamers were gradually exposed to gold nanomaterial in presence of 0.1 M NaCl in a PBS buffer over a 16-hour period according to a procedure we reported before [26,40,50]. To remove the unbound RNA, we centrifuged the solution at 13,000 rpm for 20 minutes and the precipitate was redispersed in 2 mL of the buffer solution. We have continued this process three times. To measure the number of aptamer molecules in each gold nanoparticle, after conjugation, we have treated the aptamer conjugated gold nanoparticle with 10 μM potassium cyanide to oxidize the gold nanoparticle. After that, the solution containing the released Rh6G-labeled aptamers were collected for the fluorescence analyses. The amount of Rh6G-labeled aptamers was measured by fluorescence. By dividing the total number of Rh6G-labeled aptamers by the total number of nanoparticles, we estimated that there were about 400–500 aptamers per popcorn shape gold nanoparticles. This experiment has been performed 5–6 times and average values are reported in this manuscript.

To modify the gold nanoparticle surface by amine groups (as shown in Scheme 1), we have added 30 mM cystamine dihydrochloride to 50 mL of gold nanoparticle and the solution was kept at 50° C for several hours under constant sonication. After that, the excess cystamine dihydrochloride was removed by centrifugation at 8000 rpm for several minutes. For covalent immobilization of the monoclonal anti- PSMA antibody onto the amine, we have used highly established glutaraldehyde spacer method [26,40,50]. To remove the excess antibody, we have washed aptamers and anti-PSMA anibody conjugated nanoparticles several times with PBS. To measure the number of anti-PSMA antibody molecules in each gold nanoparticles, we have performed the above process with Rh6G -labeled anti- PSMA antibody. After conjugation, we have performed exactly the same process as what we did for Rh-6G labeled aptamers. We estimated that there were about 80–100 anti-PSMA antibodies per popcorn shape gold nanoparticle. This experiment has been performed 5–6 times and average values are reported in this manuscript. During the aptamer conjugation and immobilization of the antibody, we have not noted any aggregation of gold nanoparticles as examined by TEM and UV-visible absorption spectroscopy.

Characterization of Multifunctional Gold Nanoparticle

To characterize popcorn shape gold nanoparticle conjugates with A9 aptamer and anti-PSMA antibody, we have performed DLS measurement as shown in Table 1. DLS measurement was performed using Malvern Zetasizer Nano instrument.

As shown in Table 1, popcorn shape gold nanoparticles have average size is about 28 nm, which can be seen clearly from our TEM data. The addition of A9 aptamer to the gold nanoparticle, changes the diameter to about 40 nm. This is expected due to PSMA aptamer size is around 6 nm, which increased total diameter around 12 nm. Similarly addition of anti-PSMA antibody changes the diameter is about 44 nm, which is very similar to the recent report by Liu et. al [18]. This experiment has been performed 5–6 times and average values are reported in this manuscript. Since hydrodynamic diameter of conjugated gold nanoparticle is very close for A9 aptamer conjugated gold nanoparticle and anti-PSMA antibody conjugated gold nanoparticle, we believe both aptamer and antibodies are conjugated with popcorn shape gold nanoparticle.

Cell Culture and Cellular Incubation with Multifunctional Nanoparticle

Cancer cells were grown in a 5% CO_2 incubator at 37 °C using RPMI-1640 medium (ATCC, Rockville, MD) supplemented with 10% premium fetal bovine serum (FBS)

(Lonza, Walkersville, MD) and antibiotics (10 IU/mL penicillin G and streptomycin) in 75-cm^2 tissue culture flasks. Before the experiments, the cells were re-suspended at a concentration of 1×10^6 cells/mL in PBS buffer medium. An enzyme-linked immunosorbent assay kit was used to quantify PSMA in different tested cells. Our experimental results indicated that amount of PSMA in LNCaP cell was 5.8×10^6/cells, whereas PSMA amount was only 1.6×10^3/cells in case of PC3 cell, which is comparable to the reported concentration of PSMA in different cancer cell lines [24–25,30]. Different numbers of cells were then immersed into the multifunctional popcorn shape gold nanoparticle solution for 30 min at room temperature before performing the experiment.

Surface Enhanced Raman Spectroscopy (SERS) Probe for Targeted Sensing of Cancer Cells

For SERS experiment, we have designed a SERS probe, as we have reported recently [39]. As shown in Scheme 2, we have used a continuous wavelength DPSS laser from laser glow technology (LUD-670) operating at 670 nm, as an excitation light source. This light source has a capability that can minimize whole sensor configuration. We have used InPhotonics 670 nm Raman fiber optic probe for excitation and data collection. It is a combination of 90 μm excitation fiber and 200 μm collection fiber with filtering and steering micro-optics. We have used miniaturized QE65000 Scientific-grade Spectrometer from Ocean Optics as a Raman detector. The spectral response range of this mini Raman spectrometer is 220–3600 cm^{-1}. It is equipped with TE cooled 2048 pixel CCD and interfaced to computer via a USB port. The Hamamatsu FFT-CCD detector used in the QE65000 provides 90% quantum efficiency with high signal-to-noise and rapid signal processing speed as well as remarkable sensitivity for low-light level applications. Raman spectrum was collected with Ocean Optics data acquisition SpectraSuite spectroscopy software.

Photothermal Therapy and % of live cell determination

For photothermal therapy using NIR radiation we have used a continuous wavelength portable OEM laser operating at 785 nm, as an excitation light source for 30 minutes. After that, we have used MTT test to find the amount of live cell during nanotherapy process. For this purpose, prostate cancer cells were seeded in 96-well plates (well diameter 6.4 mm) with a density of 10, 0000 cells/well and allowed to attach for 24 h at 37°C in a 5% CO$_2$ incubator, before the treatment. Cell viability was determined 1 h after photothermal treatment, using the 3-(4,5-dimethylthiazol-2-yl)-2,5-diphenyltetrazolium bromide (MTT) cell proliferation assay kit (ATCC CA# 30-1010k). This experiment has been performed 5–6 times and average values are reported in this manuscript

Time dependent In-Situ Photothermal Nano-Therapy Study using SERS Probe

For in-situ SERS intensity measurement, we have designed a portable sensor concept, as shown in Scheme 2. As we discussed before, for nano-therapy we have used a continuous wavelength OEM laser operating at 785 nm, as an excitation light source. For on time SERS measurement during therapy process, a continuous wavelength DPSS laser from laser glow technology (LUD-670) operating at 670 nm, as an excitation light source. This light source has a capability that can minimize whole sensor configuration. We have used InPhotonics 670 nm Raman fiber optic probe for excitation and data collection. It is a combination of 90 μm excitation fiber and 200 μm collection fiber with filtering and steering micro-optics. Both light sources have a capability to minimize whole sensor configuration. We have used miniaturized QE65000 scientific-grade Spectrometer from Ocean Optics as a SERS detector,

which has remarkable sensitivity for low-light level applications. This experiment has been performed 5–6 times and average values are reported in this manuscript.

Results and Discussion

Our popcorn shape gold nanoparticle based SERS approach for the detection of selective human prostate cancer cell line LNCaP is based on the fact that in the presence of cancer cell line, multifunctional popcorn shape gold nanoparticle undergo aggregation (as shown in Figure 1B). As a result, it formed several hot spots and provided a significant enhancement of the Raman signal intensity from Rh6G modified aptamers by several orders of magnitude (2.5×10^9) through electromagnetic field enhancements. For LNCaP cell line, a cancer cell has many surface epidermal growth factor prostate-specific membrane antigen receptor available for specific recognition with monoclonal anti-PSMA antibody and A9 aptamers conjugated popcorn shape gold nanoparticle. As a result, after the addition of LNCaP cell line, several nanoparticles can bind to PSMA receptors in one cancer cell, thereby producing nanoparticle aggregates (as shown in Scheme 1). Our TEM image (as shown in Figure 1B) shows clearly that multifunctional nanoparticles are strong aggregates on the surface of cancer cell. As a result, a new broad band appears around 180 nm far from their plasmon absorption band, as shown in Figure 1F. This red shift might be due to two factors. One is the change in the local refractive index on the nanoparticle surface caused by the specific binding of the multifunctional nanoparticle (NP), which binds to PSMA on the LNCaP cell surface. The other is the interparticle interaction resulting from the assembly of nanoparticles on the cell surface [11–40]. As shown in Figure 1C and 1D, our TEM image also clearly demonstrated that the HaCaT noncancerous cells and PSMA negative human prostate cancerous PC-3 cells are poorly labeled by the multifunctional nanoparticles even after 4 hours of incubation and as a result, we have not observed any new broad band corresponding to nano-aggregates (as shown in Figure 1F). As noted from Figure 1C and 1D, some popcorn shape gold nanoparticles are also found on the HaCaT noncancerous cells and PC-3 cancerous cells and it is mostly due to the nonspecific interactions and thus the nanoparticles are randomly distributed on the whole cells.

The largest Raman scattering enhancements, even single molecule SERS, have been described for molecules residing in the fractal space between aggregated colloidal nanoparticles [31–39]. This is attributed to plasmonic coupling between nanoparticles in close proximity, which results in huge local electromagnetic field enhancements in these confined junctions or SERS hot spots [31–39]. As our data clearly shows that cancer cell helps to generate hot spots through aggregation in multifunctional popcorn shape gold nanoparticle surface and as result, we have noted about eight orders of magnitude enhancement of Raman signal (as shown in Figure 1G). The Raman modes at 236, 252, 273 and 376 cm^{-1} are N-C-C bending modes of ethylamine group of the Rh6G ring and the Raman modes at 615, 778, 1181, 1349 1366,1511, 1570, 1603 and 1650 cm^{-1} are due to C-C-C ring in-plan bending, C-H out-of-plan bending, C-N stretching and C-C stretching, as we reported before [39,43]. As shown in Figure 1E, at higher concentration of cancer cell, not only multifunctional nanoparticle aggregates on cancer cell, it also helps for the formation of cancer cell clusters. To understand how the SERS assay responses with single bio-functional nanoparticle, we have also performed experiments on the addition of LNCaP cancer, with only A9 aptamers conjugated popcorn shape gold nanoparticle, only anti PSMA antibody conjugated popcorn shape gold nanoparticle, as well as multifunctional nanoparticles. Our experimental results shows that SERS enhancement is 4×10^6 times for only A9 aptamers conjugated popcorn shape gold nanoparticle, 1.5×10^7 times for only anti PSMA antibody conjugated popcorn shape gold nanoparticle and 2.5×10^9 times in the presence of multifunctional gold nanoparticle, which indicates that for early cancer detection multifunctional gold nanoparticle will be the best choice.

As shown in Figure 1E, at higher concentration of cells, not only multifunctional nanoparticle aggregates on cancer cell, it also helps in the formation of cancer cell clusters as we increase the concentration of the cell. The formation of cancer cell clusters are attributed to the fact that the aptamers and anti PSMA antibody-conjugated popcorn shape gold nanoparticles act as binding agents in between the cells to form a cellular network. When antibody from one side of the nanoparticle binds to a specific binding site on the surface of the target cancer cell, there are other antibodies on the other side of nanoparticle that could be unoccupied, thereby providing an opportunity to bind to more than one cancer cell on each nanoparticle. Nanoparticle aggregates, which make bridge between two cells, will have an opportunity to generate perfect hot spot for SERS enhancement.

The Raman enhancement, G, is measured experimentally by direct comparison as shown below [31−39],

$$G=[I_{\text{SERS}}]/[I_{\text{Raman}}] \times [M_{\text{bulk}}]/[M_{\text{ads}}]$$

where I_{SERS} is the intensity of a 1511 cm^{-1} vibrational mode in the surface-enhanced spectrum in the presence of cancer cell, and I_{Raman} is the intensity of the same mode in the bulk Raman spectrum from only Rh6G. M_{bulk} is the number of molecules used in the bulk, M_{ads} is the number of molecules adsorbed and sampled on the SERS-active substrate. All spectra are normalized for integration time. An enhancement factor estimated from the SERS signal and normal Raman signal ratio for 1511 cm^{-1} band is approximately 2.5×10^9. No significant changes in Raman frequencies are observed in comparison to the corresponding SERS and Raman bands.

To evaluate whether our assay is highly selective, we have also performed how SERS intensity changes upon the addition of HaCaT non-cancerous cell and PSMA negative human prostate cancer cell line (PC-3). As shown in Figure 1G, that SERS intensity was negligible in the presence of 10^5 HaCaT cells or when we added 10^5 PC-3 prostate cancer cells to multifunctional popcorn shape gold nanoparticles. Since both HaCaT and PC-3 cells, do not over express PSMA, there will be a weak interaction between multifunctional popcorn shape gold nanoparticle and HaCaT or PC-3 cancer cell line. Due to the lack of strong interaction, nanoparticles do not produce enough hotspots and as a result, Raman enhancement has not been observed. This contrast difference clearly demonstrates that our multifunctional popcorn shape gold nanoparticles based SERS scattering assay is highly specific for LNCaP human prostate cancer cell line and even it can distinguish between different prostate cancer cell lines.

To evaluate the sensitivity of our SERS probe, different concentrations of LNCaP human prostate cancer cell line from one stock solution were evaluated. As shown in Figure 1H and 1I, the SERS intensity is highly sensitive to the concentration of LNCaP human prostate cancer cell. Our experimental results (as shown in Figure 1H) clearly demonstrate that the sensitivity of our SERS probe is as low as 50 cells. As shown in Figure 1I, our experimental results also demonstrate that as we increase the concentration of LNCaP cancer cell above 10^5, the SERS intensity remains almost unchanged. It may be due to the fact that as we increase the concentration of LNCaP cancer cell, aggregates or cluster size increases. Since it is known that small cluster is better for hot spot formation, increasing cluster size may decrease number of hot spots and as a result, intensity decreases after certain concentration of LNCaP human prostate cancer cell.

After successful targeted sensing of LNCaP human prostate cancer cell using multifunctional popcorn shape gold nanoparticle, we performed NIR irradiation experiments

to determine whether it can be used for photo thermal nanotherapy of LNCaP cancer cell. During photothermal therapy, the light absorbed by the gold nanoparticles is transferred to the antibody, aptamer and cell environment by rapid electron-phonon relaxation in the nanoparticle followed by phonon-phonon relaxation [8–10]. In our nanotherapy experiment, we have used 80–120 mW 785 nm NIR light for 30 min using a 785 nm OEM laser. This irradiation wavelength matches with the plasmon bands of the LNCaP cancer cell conjugated popcorn shape gold nanoparticles. As shown in Figure 2, exposure to the 785 nm at 100 mW (12.5 W/cm^2) caused photo destruction of whole prostate cancer cells. TEM pictures (Figure 2D and 2E) of the irradiated cells clearly show areas of massive irreparable cell membrane disruption. After therapy, cell viability is detected by MTT test as well as using bright field inverted microscope technique. To find out the extent of cell death, we added trypan blue. Figure 2A clearly shows that cells are 100 % alive without therapy. On the other hand, Figure 2B clearly shows that most of the cancer cell is dead after 30 minutes of nanotherapy process. Our bright field inverted microscope image also clearly shows that cancer cells are deformed during nanotherapy process. This cell death following nanoparticle exposure to NIR radiation could be due to numerous factors, including nanoparticle explosion, shock waves, bubble formation, and thermal disintegration. As shown in Figure 2D and 2E, clear bubble formation (indicated by purple circle) when multifunctional popcorn shape gold nanoparticle conjugated LNCaP cell was exposed to 100 mW, 785 nm NIR continuous-wave radiation. Temperature measurement indicates that the temperature increases to 48° C during the nanotherapy process. As shown in Figure 2H, our time interval MTT test indicates that within 30 minutes most of the cancer cell died. We have also performed same tests with PSMA negative prostate cancerous (PC-3) and non-cancerous (HaCa T) cells (as shown in Figure 2G) and we found that the cancer cells required less than half the laser energy (8 W/cm2) for photothermal lysis in comparison to the normal cells (20 W/cm2). Now, to understand how good is the photo-thermal performance of our nano popcorn shape gold nanoparticles, we also performed same photothermal experiment with multifunctional gold nanorod (σ = 2.3) using 100 mW, 785 nm NIR continuous-wave radiation. We have maintained the concentration of gold nanomaterials in such way that after aggregation in the presence of LNCaP cell, the absorption coefficient at 785 nm is around 0.5. Figure 2H, clearly shows that photo-thermal response for nano-popcorn based gold nanoparticle is slightly better or comparable to well studied gold nanorod. Though their photothermal response is similar, in nano-popcorn several narrow nanoscaled corners are capable of focusing the field at their apexes, which will provide huge enhancement of SERS signal, and as a result, nano-popcorn will be better SERS substrate than gold nanorod.

The electron–phonon relaxation process is size and shape independent and results in temperature rises on the order of a few tens of degrees [8–10,14–16,58–59]. Depending on the extent of heat generated during photothermal process, several subsequent processes can occur [8–10,14–17,58–59]: (1) The lattice cools off by passing its heat to the surrounding medium via phonon–phonon relaxation, which produces sufficient heating for the destruction of chemically attached cancer cells. (2) The lattice heat content is sufficient enough to lead to particle structural changes such as nanoparticle fragmentation. (3) Due to electronic coupling of the surface gold-sulfur bond vibrations with the nanoparticle surface phonons, there is a possibility of the gold-sulfur bond breaking. As a result, dye modified aptamers are released from surface. First process will lead to irreversible cell destruction through protein denaturation and coagulation as well as cell membrane destruction. As shown in Figure 2D and 2E, bubble formation around gold nanoparticles occur during nanotherapy process, which may impose mechanical stress, resulting in cell damage. During the second process, there is a possibility of nanoparticle structural change. To understand whether this process is occurring in this case, we have performed time dependent TEM study and absorption spectral measurements during nano-therapy process. As shown in

Figure 2C, after 10 minutes of photothermal process, there is a clear deformation of the nano-propcorn structure. Our data clearly show that tips are mostly vanished and since the tips are capable of focusing the field at their apexes, which provides sufficient field of SERS enhancement, SERS intensity should decrease for this deformation process. Our TEM data after 20 and 30 minutes nano-therapy process show huge irreparable damage of cancer cell surfaces and bubble formation and as a result, it is very difficult to find out about the fate of nano-structure by TEM study. To have a clear picture, we recorded absorption spectra before and after photothermal therapy process. As shown in Figure 1F, the aggregated nanoparticle concentration decreases after therapy and we see a strong broad band between 500–600 nm region, which is mainly due to the deformed nanostructure, formed during therapy process. Based upon this SERS intensity change due to the thermal deformation of gold nano-structure during photothermal process, nanotherapy response can be monitored.

Now during third process, there is a possibility of breaking the gold-sulfur bond. As a result, dye modified aptamers are released from the surface. Due to this release, the separation distance between gold nanoparticle and Rh6G dye changes abruptly and this destroys SERS signal from Rh-6G. As shown in Figure 3A, we observed a very distinct SERS intensity change after 30 minutes of photothermal therapy. This distinct SERS intensity change can be mainly due to two factors and these are 1) the distance between gold nanoparticle and Rh-6G dye changes during nano-therapy and 2) change in the morphology of gold nanoparticle. To understand whether our assumptions on gold nanoparticle structural change and dye modified aptamer release from surface during nano-therapy are possible mechanisms, we have also performed nanoparticle surface energy transfer (NSET) experiment using fluorescence dye Cy3-labeled A9 aptamer and anti-PSMA antibody attached popcorn shape gold nanoparticle attached LNCaP cell nano-therapy experiment. Details of the NSET experimental set up have been reported recently by our group [42,44,47]. In this case, we have used 532 nm as an excitation source to monitor the NSET intensity change during therapy process. As shown in Figure 3B, when only Cy3 dye (100 nM) was adsorbed on gold nanoparticle, fluorescence signal was quenched about 100%. In this condition, since the acceptor nanoparticle and donor organic dyes are brought into proximity, there are dipole-surface type energy transfer from dye molecular dipole to nanometal surface, which known as NSET [42,44,47]. Since before therapy, Cy3-labeled A9 aptamers are attached with gold nanoparticle, the fluorescence from Cy3-labelled aptamers is more than 80% quenched by gold nanoparticles and as a result, we observe very little fluorescence signal (as shown in Figure 3B). In this condition, since the acceptor nanoparticle and donor organic dyes are about 6 nm far, there are very strong dipole-surface type energy transfer from dye molecular dipole to nanometal surface, as a result more than 80% fluorescence was quenched. Now, during therapy if dye modified aptamers are released from surface and gold nanoparticle, this distance change will generate huge fluorescence signal. Our experimental results, as shown in Figure 3B, clearly shows that NSET signal mostly restored after the nano-therapy, which confirms that the distance between nano-surface and dye are changing during therapy process and it is mainly due to the breaking of Au-S bond. Recently Poon et. al. [58] also reported photothermal release of DNA through Au-S bond breaking, which also confirms that Au-S bond breaking can be a possible mechanism. Now to understand whether all dye attached aptamers are released during therapy process, after therapy process, we have treated the aptamer conjugated gold nanoparticle attached cancer cell with 100 μM potassium cyanide to oxidize the gold nanoparticle and as a result, all dye molecules will be released to the solution. As shown in Figure 3B, our result clearly shows that fluorescence signal increases only 20% after the addition of cyanide, which indicates that after therapy a nanoparticle has only around 80 dye attached aptamers. As a result, our experimental result clearly shows that the third process can be the possible path for the decrease in SERS intensity during nano-therapy. As we have discussed before, a multifunctional gold nanoparticle has 400–500 dye attached aptamers.

Now, during the conjugation of gold nanoparticle and cancer cell line, most of the aptamers will be used for conjugation with cancer cell line and some of them will be free. We believe that during therapy process, since cancer cell membrane is damaged, aptamer which is conjugated to cancer cell will be removed easily. As a result, we see 80% dye released during the therapy process. Figure 3B also shows that fluorescence signal due to the addition of 100 μM potassium cyanide before therapy and after therapy is very similar, which clearly shows that there is no photo bleaching of Cy3 dyes during therapy process.

Next, to understand whether antibody is also released during therapy process, we have performed NSET experiment using Cy3-labeled anti-PSMA antibody and A9 aptamer coated popcorn shape gold nanoparticle attached LNCaP cell nano-therapy experiment. As shown in Figure 3C, our experimental results clearly shows that NSET signal mostly restored after the nano-therapy, which confirms that the distance between nano-surface and dye attached antibody are changing during therapy process. Now to understand how many antibody are released during therapy process, after therapy process, we have treated the antibody conjugated gold nanoparticle attached cancer cell with 100 μM potassium cyanide. As shown in Figure 3C, our result clearly shows that fluorescence signal increases by only 40% after addition of cyanide which indicates that around 60% antibodies are released during therapy process. Figure 3C also shows that fluorescence signal due to the addition of 100 μM potassium cyanide before therapy and after therapy is very similar, which clearly shows that there is no photo bleaching of Cy3 dyes during therapy process.

After that, to understand whether the cell is necessary to release aptamers during laser exposing process in our experimental condition, we have exposed Cy3-labeled A9 aptamers and anti-PSMA antibody coated popcorn shape gold nanoparticle to 100 mW, 785 nm NIR continuous-wave radiation for 30 minutes and monitored time dependnet NSET intensity. As shown in Figure 3D, our experimental results clearly show that NSET signal changes very little, which confirms that the distance between nano-surface and dye attached multifunctional nanoparticle is not changing sufficiently during therapy process. Now, to understand how many aptamers are released during therapy process, after therapy process, we have treated the multifunctional nanoparticle with 100 μM potassium cyanide. As shown in Figure 3D, our result clearly shows that fluorescence signal increases by about 95% after addition of cyanide which indicates that less than 5% aptamers are released during laser treatment process. Figure 3D also shows that the fluorescence signal due to the addition of 100 μM potassium cyanide before and after laser treatment is very similar, which clearly shows that there are no photo bleaching of Cy3 dyes during therapy process. Absence of Au-S bond breaking with out cancer cell line is may be due to the following facts. 1) Several articles demonstrated that antibody-assisted aggregation of Au nanoparticles on cell membranes or in intracellular environments led to the high enhancement of photothermal performance [60–63]. Since in our case, aggregates were formed only in presence of cancer cell, which have strong absorption at 785 nm, photothermal therapy effect should be highly efficient in the presence of aggregates; 2) Multifunctional popcorn shape gold nanoparticle exhibits very little absorption at 785 nm.

Next, we have performed in-situ time dependent SERS measurement experiment during nanotherapy process to understand whether our SERS assay can monitor the nanotherapy process, using SERS intensity change. For in-situ SERS intensity measurement, we have designed a portable sensor, as we described before and shown in Scheme 2. As we discussed before, for nano-therapy we have used a continuous wavelength OEM laser operating at 785 nm, as an excitation light source. Figure 3E, demonstrates how the SERS intensity decreases during therapy process. We have recorded the data in 2 minutes interval during the therapy process. Our in-situ time dependent measurement clearly shows that as the nano-therapy progresses, the SERS intensity decreases. To understand whether there is any correlation

between % of LNCaP prostate cancer cell death and SERS intensity change, we have plotted % of cell viability and SERS intensity change. As shown in Figure 3F, we see a nice linear plot between % of LNCaP prostate cancer cell viability and SERS intensity change where $R(t)$ is the SERS intensity at time t, during nanotherapy and $R(0)$ is the initial SERS intensity, before therapy. Our result clearly shows that it is possible to use SERS assay for the measurement of in-situ nano-therapy response during therapy process for LNCaP prostate cancer cell line.

To understand whether our technique is versatile, we have also tested whether our SERS based approach can be applicable to monitor nanotherapy process of breast cancer cell line. For this purpose, a well characterized breast cancer SK-BR-3 cell line, which overexpresses epidermal growth factor receptor HER2/c-erb-2/Neu has been used. For specific recognition of SK-BR-3 cell line we have modified pop-corn shape gold nanoparticle with monoclonal anti-HER2/c-erb-2 antibody and Rh6G modified S6 aptamer. For photothermal therapy we have exposed the multifunctional popcorn shape gold nanoparticle attached SK-BR-3 cell to 100 mW, 785 nm laser light for 30 minutes and used MTT test to find the cell viability. We have also performed in-situ time dependent SERS measurement experiment during nanotherapy process using the same procedure as we have done for LNCaP prostate cancer. As shown in figure 3G, our in-situ time dependent measurement clearly shows that as the SK-BR-3 cell line nano-therapy progresses, the SERS intensity decreases, similar to what we observed for LNCaP prostate cancer cell line. Now, to find whether there is any correlation between % of cell death and SERS intensity change, we have plotted % of Sk-BR-3 cell viability and SERS intensity change. Figure 3H shows a nice linear plot between % of SK-BR-3 breast cancer cell viability and SERS intensity change. Our result clearly demonstrates that it is possible to use SERS assay for the measurement of in-situ nano-therapy response during therapy process for different cancer cell lines.

To understand whether the SERS intensity change depends on the formation of conjugation between multifunctional gold nanoparticle and cancer cell line, we have performed time dependent SERS intensity change during photo-thermal process for PC-3 and HACaT cell line in the presence of Rh-6G modified A9 aptamer and anti-PSMA antibody coated popcorn shape gold nanoparticle. As we discussed before, for multifunctional gold nanoparticle not conjugated well with PC-3 and HaCaT cell line, as a result we do not expect much nano-therapy activity for these cell lines when they were exposed to 100 mW, 785 nm laser light for 30 minutes. As shown in Figure 3I, SERS intensity changes little in the case of PC-3 and HaCaT cell line, whereas SERS intensity changes abruptly for LNCaP cell line. Our data clearly demonstrates that our SERS assay for nano-therapy monitoring is highly selective and nanoparticle conjugation with cancer cell line is necessary to monitor therapy process. Looking into the future, we expect that these SERS sensor developments will have important implications in the development of better bioassay for monitoring tumor response to therapy during the photothermal nanotherapy process in clinical samples.

Conclusion

In conclusion, in this article, we have demonstrated multifunctional popcorn shape gold nanotechnology-driven surface enhanced Raman scattering (SERS) assay for targeted sensing, nanotherapy treatment and in-situ monitoring photothermal nanotherapy response during the therapy process. We have shown that in the presence of LNCaP human prostate cancer cell, multifunctional popcorn shape gold nanoparticle forms several hot spots and provided a significant enhancement of the Raman signal intensity from Rh6G modified aptamers by several orders of magnitude (2.5×10^9) through electromagnetic field enhancements. Our experimental data with HaCaT non-cancerous cell line, as well as with PSMA negative PC-3 prostate cancer cell line clearly demonstrates that our SERS assay is

highly sensitive to LNCaP and it was able to distinguish from other breast cancer cell line. Our experiment indicates that this bioassay is highly sensitive with detection ability of up to 50 cancer cells. We have clearly demonstrated that when popcorn shape multifunctional gold nanoparticles are attached to cancerous cells, the localized heating that occurs during NIR irradiation is able to cause irreparable cellular damage. This popcorn shape gold nanotechnology based assay is rapid, takes about 30 minutes from cancer cell binding to detection and destruction of the cell. Our data clearly show that photo-thermal response for nano-popcorn based gold nanoparticle is slightly better or comparable to well studied gold nanorod.

Our in-situ time dependent experimental results clearly demonstrate that as the nano-therapy progresses, the SERS intensity increases and as a result, by monitoring SERS intensity change, one can monitor the photo thermal therapy response in time. Our experimental data indicate a nice linear plot between % of cancer cell death and SERS intensity change, which clearly shows that it is highly feasible to use SERS assay for the measurement of in-situ nano-therapy response during therapy process, which is critical to providing effective treatment of cancer. Although we have shown promising advances in multifunctional popcorn shape gold nanoparticle based SERS assay, we still need a much greater understanding of how to control surface architecture in order to stabilize and maximize the assay response. Though our experimental results confirm that multifunctional nanoparticle based assay will be very good for early stage cancer cell detection, due to the presence of PSMA in different normal tissues, there are chances for false positive signals. Since PSMA level for cancer cell is usually much higher than normal tissues, a detailed study on the PSMA level in different normal tissues and cancerous cell are necessary, before this assay can be used for real life applications. After optimization of different parameters, we believe that this nanotechnology driven assay could have enormous potential application in rapid, on-site targeting cancer cell, nano therapy treatment and monitoring nanotherapy process which is critical to providing effective, noninvasive treatment of cancer.

Acknowledgments

References

1. Bray F, Møller B. Nature Reviews Cancer. 2006; 6:63–74.

2. http://www.who.int/cancer/en

3.
http://www.cancer.org/docroot/cri/content/
cri_2_4_1x_what_are_the_key_statistics_for_prostate_cancer_36.asp

4. http://www.cdc.gov/cancer/prostate

5. http://www.cdc.gov/cancer/dcpc/data/men.htm

6. Shewach DS, Kuchta RD. Chem Rev. 2009; 109:2859–2861. [PubMed: 19583428]

7. Deutscher SL. Chem Rev. 2010; 110:196–3211.

8. Louie A. Chem Rev. 2010; 110:3146–3195. [PubMed: 20225900]

9. Ferrari M. Nature Reviews Cancer. 2005; 5:161–171.

10. Scheinberg DA, Villa CH, Escorcia FE, McDevitt RM. Nature Reviews Clinical Oncology. 2010; 7:266–276.

11. Lal S, Clare SE, Halas NJ. Acc Chem Res. 2008; 41:1842–1851. [PubMed: 19053240]

12. Jain PK, Huang X, El-Sayed IH, El-Sayed MA. Acc Chem Res. 2008; 41:1578–1586. [PubMed: 18447366]

13. Cheon J, Lee J-H. Acc Chem Res. 2008; 41:1630–1640. [PubMed: 18698851]

14. Peer D, Karp JM, Hong S, Farokhzad OC, Margalit R, Langer R. Nature Nanotechnology. 2007; 2:751–760.

15. Sarkar B, Dosch J, Simeone DM. Chem Rev. 2009; 109:3200–3208. [PubMed: 19522504]

16. Nam J, Won N, Jin H, Chung H, Kim S. J Am Chem Soc. 2009; 131:13639–13645. [PubMed: 19772360]

17. Yu J, Javier D, Yaseen MA, Nitin N, Richards-Kortum R, Anvari B, Wong MS. J Am Chem Soc. 2010; 132:1929–1938. [PubMed: 20092330]

18. Liu X, Dai Q, Austin L, Coutts J, Knowles G, Zou J, Chen H, Huo Q. J Am Chem Soc. 2008; 130:2780–2782. [PubMed: 18257576]

19. Agasti SS, Chompoosor A, Chang-Cheng Y, Ghosh P, Kim CK, Rotello VM. J Am Chem Soc. 2009; 131:5728–5729. [PubMed: 19351115]

20. Sha MY, Xu H, Natan MJ, Cromer R. J Am Chem Soc. 2008; 130:17214–17215. [PubMed: 19053187]

21. Lutz BR, Dentinger CE, Nguyen LN, Sun L, Zhang J, Allen AN, Chan S, Knudsen BS. ACS Nano. 2008; 2:2306–2314. [PubMed: 19206397]

22. Stoeva SI, Lee JS, Smith JE, Rosen ST, Mirkin CA. J Am Chem Soc. 2006; 128:8378–8379. [PubMed: 16802785]

23. Huang X, El-Sayed IH, Qian W, El-Sayed MA. J Am Chem Soc. 2006; 128:2115–2120. [PubMed: 16464114]

24. Javier DJ, Nitin N, Levy M, Ellington A, Richards-Kortum R. Bioconjugate Chem. 2008; 19:1309–1312.

25. Sardana G, Jung K, Stephan C, Diamandis EP. J Proteome Res. 2008; 7:3329–3338. [PubMed: 18578523]

26. Lu W, Arumugam SA, Senapati D, Singh AK, Arbneshi T, Khan SA, Yu H, Ray PC. ACS Nano. 2010; 4:1739–1749. [PubMed: 20155973]

27. Huang Y-F, Liu H, Xiong X, Chen Y, Tan W. J Am Chem Soc. 2009; 131:17328–17334. [PubMed: 19929020]

28. Qian X, Zhou X, Nie S. J Am Chem Soc. 2008; 130:14934–14935. [PubMed: 18937463]

29. Jain PK, Qian W, El-Sayed MA. J Am Chem Soc. 2006; 128:2426–2433. [PubMed: 16478198]

30. Gordon IO, Tretiakova MS, Noffsinger AE, Hart J, Reuter VE, Ahmadie HA. Modern Pathology. 2008; 21:1421–1427. [PubMed: 18839017]

31. Brown SD, Nativo P, Smith JA, Stirling D, Edwards PR, Venugopal B, Flint DJ, Plumb JA, Graham D, Wheate NJ. J Am Chem Soc. 2010; 132:4678–4684. [PubMed: 20225865]

32. Camden JP, Dieringer JA, Zhao J, Van Duyne RP. Acc Chem Res. 2008; 41:1653–1661. [PubMed: 18630932]

33. Brus L. Acc Chem Res. 2008; 41:1742–1749. [PubMed: 18783255]

34. Moskovits M. Rev Mod Phys. 1985; 57(3):783–826.

35. Camden JA, Dieringer JA, Wang Y, Masiello DJ, Marks LD, Schatz GC, Van Duyne RP. J Am Chem Soc. 2008; 130:12616–12617. [PubMed: 18761451]

36. Barhoumi A, Zhang D, Tam F, Halas NJ. J Am Chem Soc. 2008; 130:5523–5529. [PubMed: 18373341]

37. Laurence TA, Braun G, Talley C, Schwartzberg A, Moskovits M, Reich N, Huser T. J Am Chem Soc. 2009; 131:162–169. [PubMed: 19063599]

38. Bonham AJ, Braun G, Pavel I, Moskovits M, Reich NO. J Am Chem Soc. 2007; 129:14572–14573. [PubMed: 17985912]

39. Dasary SSR, Singh AK, Senapati D, Yu K, Ray PC. J Am Chem Soc. 2009; 131:13806–13812. [PubMed: 19736926]

40. Wang S, Singh AK, Senapati D, Neely A, Yu H, Ray PC. Chem A Eur J. 2010; 16:5600–5606.

41. Darbha GK, Singh AK, Rai US, Yu E, Yu H, Ray PC. J Am Chem Soc. 2008; 130:8038. [PubMed: 18517205]

42. Griffin J, Singh AK, Senapati D, Rhodes P, Mitchell K, Robinson B, Yu E, Ray PC. Chem Eur J. 2009; 15:342–351.

43. Tiwari V, Tovmachenko O, Darbha GK, Hardy W, Singh JP, Ray PC. Chem Phys Lett. 2007; 446:77–82.

44. Griffin J, Ray PC. J Phys Chem B, (Letter). 2008; 112:11198–11201.

45. Yun CS, Javier A, Jennings T, Fisher M, Hira S, Peterson S, Hopkins B, Reich NO, Strouse GF. J Am Chem Soc. 2005; 127:3115–3119. [PubMed: 15740151]

46. Skewis LR, Reinhard BM. Nano Lett. 2008; 8:214–220. [PubMed: 18052230]

47. Darbha GK, Ray A, Ray PC. ACS Nano. 2007; 3:208–214. [PubMed: 19206651]

48. Neely A, Perry C, Varisli B, Singh AK, Arbneshi T, Senapati D, Kalluri JK, Ray PC. ACS Nano. 2009; 3:2834–2840. [PubMed: 19691350]

49. Mallouk TE, Yang P. J Am Chem Soc. 2009; 131:7937–7939. [PubMed: 19507897]

50. Singh AK, Senapati D, Wang S, Griffin J, Neely A, Candice P, Naylor KM, Varisli B, Kalluri JR, Ray PC. ACS Nano. 2009; 3:1906–1912. [PubMed: 19572619]

51. Lorenzo LR, Javier F, Abajo G, Liz-Marzn LM. J Phys Chem C. 2010; 114:7336–7340.

52. Khoury CG, Vo-Dinh T. J Phys Chem C. 2008; 112:18849–18859.

53. Huang YF, Chang HT, Tan W. Anal Chem. 2008; 80:567–572. [PubMed: 18166023]

54. Lilja H, Ulmert D, Vickers AJ. Nature Reviews Cancer. 2008; 8:268–278.

55. Madu, Chikezie O.; Yi, Lu. J Cancer. 2010; 1:150–177. [PubMed: 20975847]

56. Nikoobakht B, Wang J, El-Sayed MA. Chem Phys Lett. 2002; 366:17–23.

57. Orendorff CJ, Murphy CJ. J Phys Chem B. 2006; 110:3990–3994. [PubMed: 16509687]

58. Poon L, Zandberg W, Hsiao D, Erno Z, Sen D, Gates BD, Branda NR. ACS Nano. 2010 (ASAP Article).

59. Wijaya A, Schaffer SB, Pallares IG, Schifferli KH. ASC Nano. 2009; 3:80–86.

60. Lapotko D, Lukianova E, Potapnev M, Aleinikova O, Oraevsky A. Cancer Lett. 2006; 239:36. [PubMed: 16202512]

61. Govorov AO, Richardson HH. Nano Today. 2007; 2:30.

62. Richardson HH, Carlson MT, Tandler PJ, Hernandez P, Govorov AO. Nano Lett. 2009; 9:1139. [PubMed: 19193041]

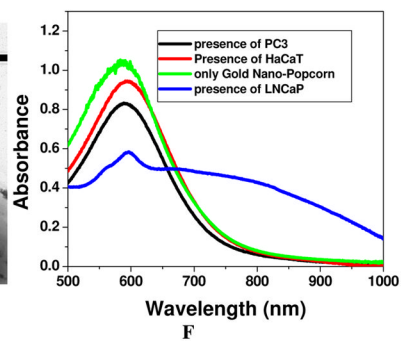63. Wang S, Chen KJ, Wu TH, Wang H, Lin WY, Ohashi M, Chiou PY, Tseng HR. Angew Chem Int Ed. 2010; 49:3777–3781.
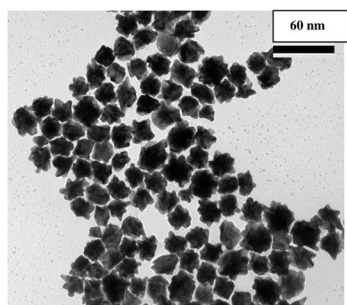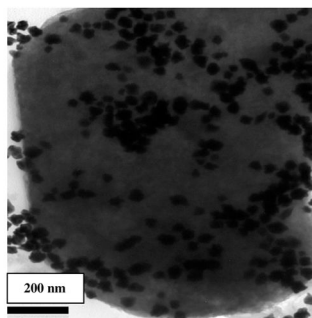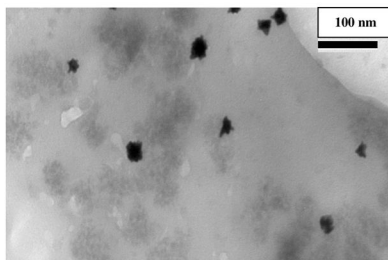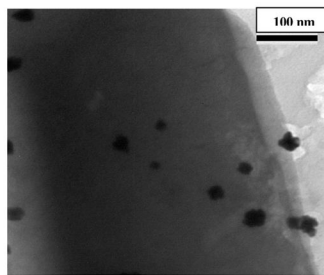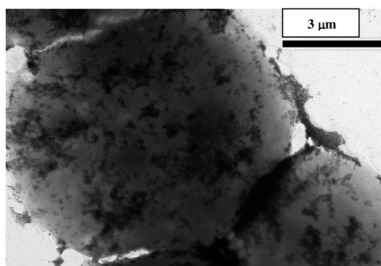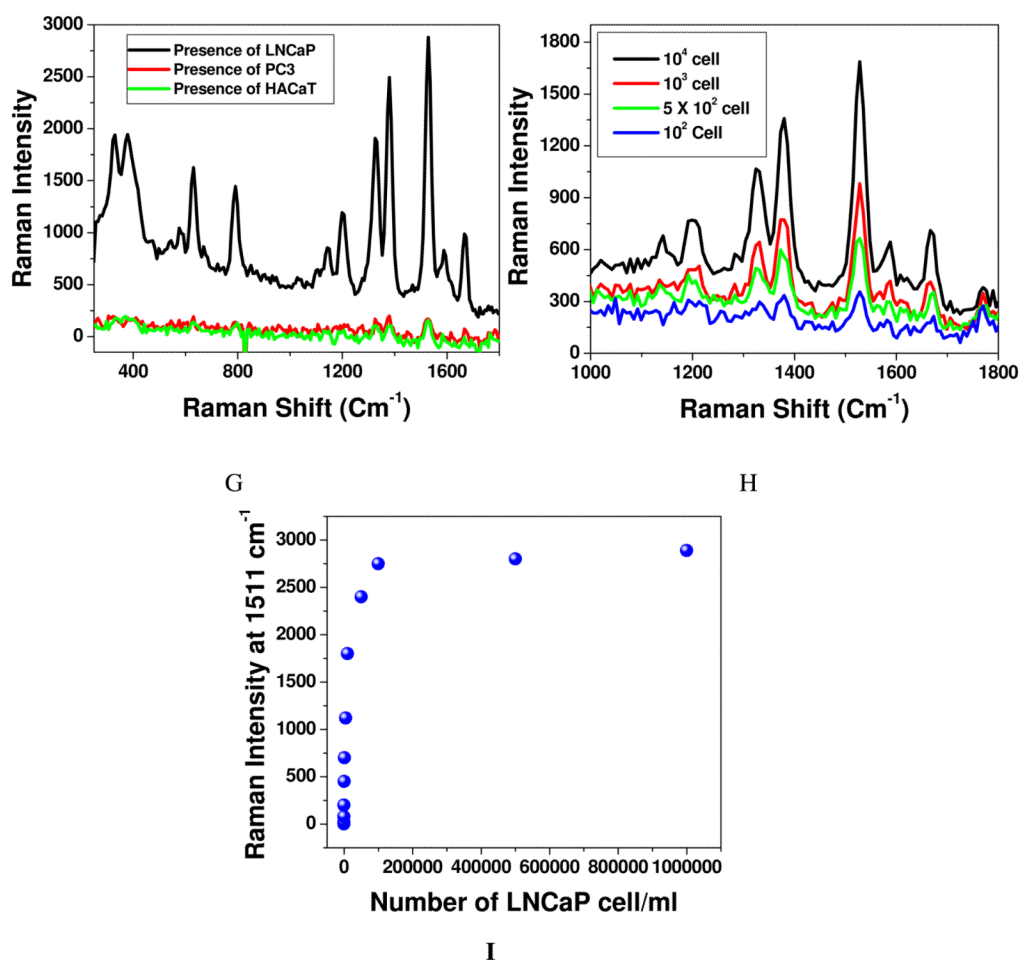
Figure 1.
A) TEM image showing anti PSMA antibody and A9 RNA aptamer conjugated popcorn shape gold nanoparticles before the addition of cancer cell line. B) TEM image demonstrating aggregation of multifunctional popcorn shape gold nanoparticles after the addition of 10^4 human prostate cancer LNCaP cells/mL for 30 minutes. C) TEM image demonstrating about no aggregation after the addition of 10^5 HaCaT cells/ml on multifunctional popcorn shape gold nanoparticles for 4 hours, where nanoparticles are randomly distributed on the whole cells. D) TEM image showing very little or about no aggregation after the addition of 10^5 PSMA negative human prostate cancerous PC-3 cells/ ml on multifunctional popcorn shape gold nanoparticles for 4 hours. E) TEM image shows the formation of cancer cell clusters in presence of 10^6 human prostate cancer LNCaP cells/ ml. F) Absorption profile showing variation of multifunctional popcorn shape gold nanoparticles due to the addition of different cancerous and non-cancerous cells. The strong long wavelength band in the visible region (λ_{PR} = 580 nm) is due to the oscillation of the conduction band electrons. New band appearing around 780 nm, due to the addition of LNCaP cell, demonstrates the aggregation of gold nanoparticles. It has also been demonstrated that the HaCaT noncancerous cells and PSMA negative human prostate cancerous PC-3 cells are poorly labeled by the nanoparticles and as a result, we have not observed any new broad band corresponding to nano-aggregates G) Plot demonstrating SERS enhancement and selectivity of our multifunctional popcorn shape gold nanoparticles based SERS assay. Raman intensity enhances 2.5×10^9 times upon the addition of 4.8×10^4

LNCaP cells/ml human prostate cancerous cells. Whereas Raman scattering intensity remains unchanged upon the addition of 10^6 PC-3 cells/ml, PSMA negative human prostate cancerous cells and 10^6 HaCaT cells/ml, human skin nan-cancerous cells. H) Plot demonstrating SERS scattering intensity changes upon the addition of different concentrations (number of cells/ml) of LNCaP human prostate cancerous cells to multifunctional popcorn shape gold nanoparticle. I) Plot demonstrating how Raman intensity at 1511 cm^{-1} changes upon the addition of different concentration (cell/ml) of LNCaP prostate cancer cell.
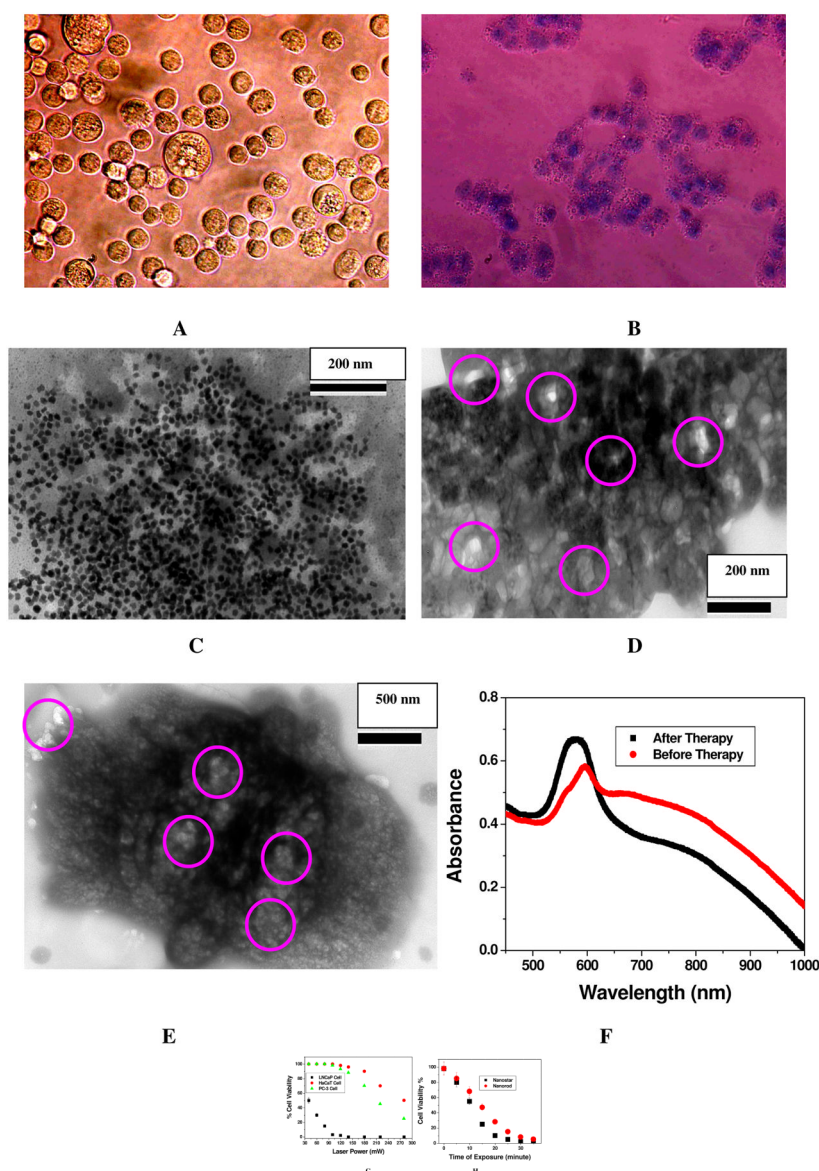
Figure 2.
A,B) Bright field inverted microscope images of multifunctional popcorn shape gold nanoparticle conjugated LNCaP prostate cancer cells, A) Before therapy, B) After therapy for 30 minutes and after stained with Trypan Blue. C) TEM image showing deformation of nano-popcorn structure after popcorn shape gold nanoparticle conjugated LNCaP cells were exposed to 100 mW, 785 nm NIR continuous-wave radiation for 10 minutes, D) TEM image showing structure deformation and irreparable damage of cancer cell surfaces after 20 minutes radiation, purple circles are showing bubble formation. E) TEM image demonstrating irreparable damage of cancer cell surfaces when multifunctional popcorn shape gold nanoparticle conjugated LNCaP cells were exposed to 100 mW, 785 nm NIR continuous-wave radiation for 30 minutes, purple circles are showing bubble formation. F) Absorption profile demonstrating nanoparticle structural change after nano-therapy process. G) Plot showing cell viability measured by MTT test after popcorn shape gold nanoparticle conjugated LNCaP cells, PC-3 and HaCaT cells were exposed to 785 nm NIR continuous-wave radiation at different power dose. H) Plot demonstrated a comparison on photothermal
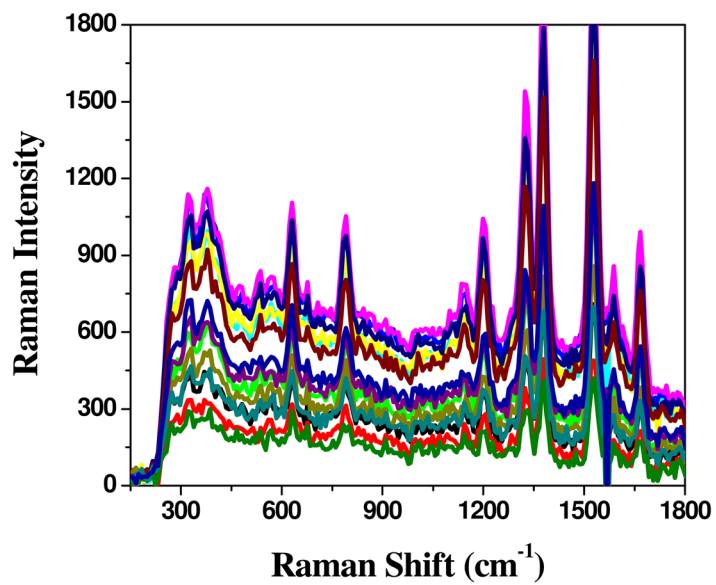
therapy response between well characterized gold nanorod and popcorn shape gold nanoparticle, when multifunctional nanoparticle conjugated LNCaP cells are exposed to 100 mW 785 nm NIR continuous-wave radiation for different times.
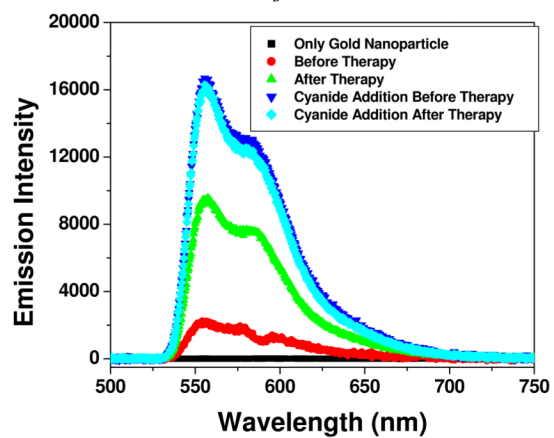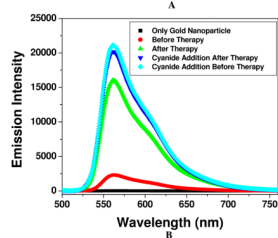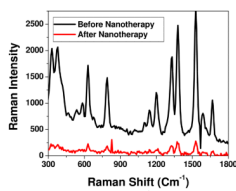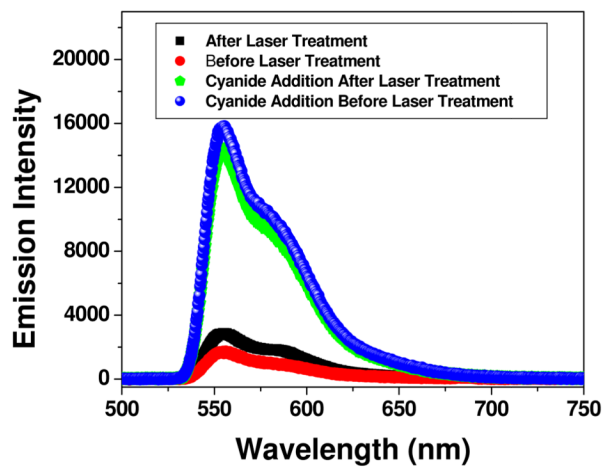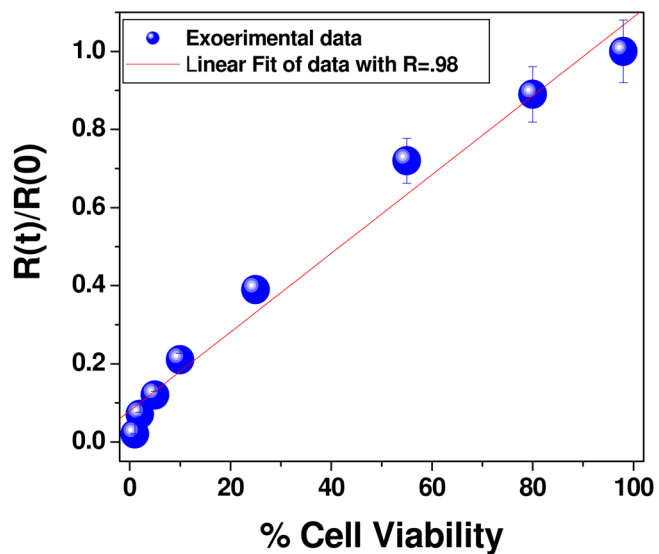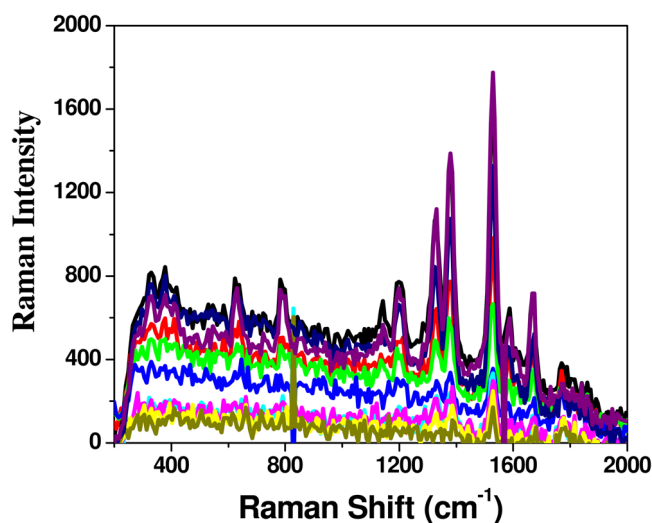
E
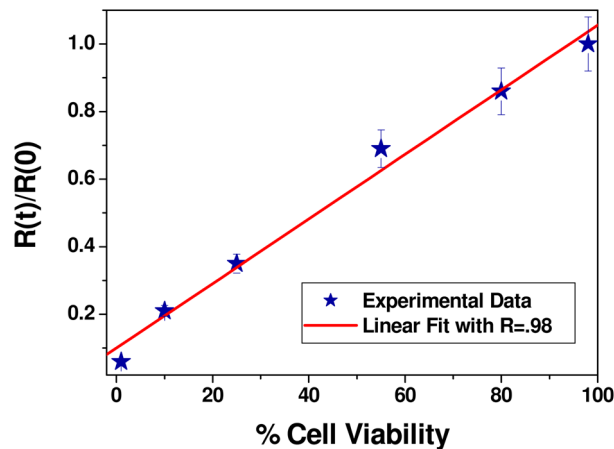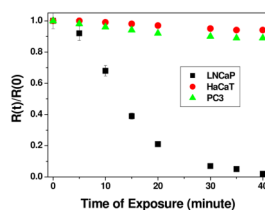


F

G

H

I

Figure 3.
A) Demonstrating surface-enhanced Raman spectral change from Rh-6G modified A9 aptamer and anti-PSMA antibody coated popcorn shape gold nanoparticles conjugated LNCaP cells, before and after nanotherapy. B) NSET intensity change before and after photothermal therapy, when Cy3 modified A9 aptamer and anti-PSMA antibody coated popcorn shape gold nanoparticle conjugated LNCaP cell was exposed to 100 mW, 785 nm NIR continuous-wave radiation for 30 minutes. Plot also demonstrates how NSET intensity changes due to the addition of cyanide in both cases before and after therapy, which destroys

the gold nanostructure completely. Similarly plot also shows that when only Cy3 dye (100 nM) was adsorbed on gold nanoparticle, fluorescence signal was quenched about 100%. C) NSET intensity change before and after photothermal therapy, when Cy3 modified anti-PSMA antibody and A9 aptamer coated popcorn shape gold nanoparticle conjugated LNCaP cell was exposed to 100 mW, 785 nm NIR continuous-wave radiation for 30 minutes. Plot also demonstrates how NSET intensity changes due to the addition of cyanide in both cases before and after therapy, which destroys the gold nanostructure completely. Similarly, plot also shows that when only Cy3 dye (100 nM) was adsorbed onto gold nanoparticle, fluorescence signal was quenched almost by 100%. D) NSET intensity change before and after laser treatment, when Cy3 modified A9 aptamer and anti-PSMA antibody coated popcorn shape gold nanoparticle was exposed to 100 mW, 785 nm NIR continuous-wave radiation for 30 minutes. Plot also demonstrates how NSET intensity changes due to the addition of cyanide ion both cases before and after laser treatment, which destroys the gold nanostructure completely. E) Plot demonstrating time dependent SERS intensity decrease during nanotherapy progress of LNCaP prostate cancer cell. SERS intensity measurements have been performed at every two minutes interval during therapy process for 30 minutes. F) Plot showing linear relationship between % of LNCaP cell viability and SERS intensity change, when multifunctional popcorn shape gold nanoparticle conjugated LNCaP cells were exposed to 100 mW, 785 nm NIR continuous-wave radiation for 30 minutes. G) Plot demonstrating time-dependent SERS intensity decrease during nanotherapy progress for SK-BR-3 breast cancer cell line, when monoclonal anti-HER2/c-erb-2 antibody and Cy3 modified S6 aptamer conjugated popcorn shape gold nanoparticle are attached on SK-BR-3 cell line. SERS intensity measurements have been performed at every two minutes interval during therapy process for 30 minutes. H) Plot showing linear relationship between % of SK-BR-3 cell viability and SERS intensity change, when multifunctional popcorn shape gold nanoparticle conjugated SK-BR-3 cells were exposed to 100 mW, 785 nm NIR continuous-wave radiation for 30 minutes. I) Plot demonstrating SERS intensity change when multifunctional popcorn shape gold nanoparticle conjugated LNCaP, PC-3 and HaCaT cells were exposed to different power 785 nm NIR continuous-wave radiation for 30 minutes.
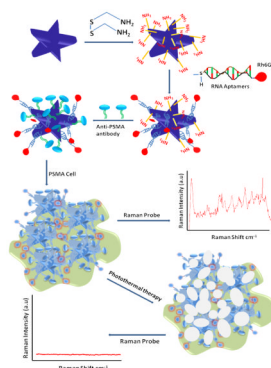
Scheme 1.
Schematic representation shows the synthesis of monoclonal anti-PSMA antibody and A9 RNA aptamers-conjugated popcorn shape gold nanoparticles. Third step shows schematic representation of multifunctional popcorn shape gold nanoparticle based sensing of LNCaP breast cancer cell line.
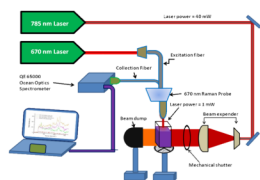
Scheme 2.
Schematic presentation for time-resolved SERS set up we have used for in-situ measurement of SERS intensity during nanotherapy.

Table 1

Size of popcorn shape gold nanoparticle before and after conjugation with aptamer and antibody

Material	Hydrodynamic Diameter
Only popcorn shape gold nanoparticle	28 nm ± 2 nm
A9 aptamers conjugated popcorn shape gold nanoparticle	40 nm ± 2 nm
Anti PSMA antibody conjugated popcorn shape gold nanoparticle	44 ± 2 nm
Multifunctional popcorn shape gold nanoparticle	43 ± 3 nm